Journal Pre-proof

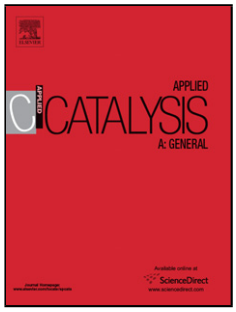

Dehydrogenation of 1-butene with CO_2 over VO_x supported catalysts

K. Iffländer (Investigation) (Methodology) (Visualization) (Writing - original draft)<ce:contributor-role>Writing -review and editing), R. Eckelt (Investigation) (Resources), H. Lund (Investigation) (Resources), C. Kreyenschulte (Investigation) (Resources), S. Bartling (Investigation) (Resources), A. Wotzka, N. Steinfeldt (Supervision) (Writing - original draft) (Writing - review and editing)

PII: S0926-860X(20)30241-6

DOI: https://doi.org/10.1016/j.apcata.2020.117648

Reference: APCATA 117648

To appear in: *Applied Catalysis A, General*

Received Date: 21 February 2020

Revised Date: 1 May 2020

Accepted Date: 18 May 2020

Please cite this article as: { doi: https://doi.org/

Dehydrogenation of 1-butene with CO_2 over VO_x supported catalysts

K. Iffländer, R. Eckelt, H. Lund, C. Kreyenschulte, S. Bartling, A. Wotzka, N. Steinfeldt

Leibniz-Institut für Katalyse e. V., Albert-Einstein-Str. 29a, 18059 Rostock, Germany

Corresponding author:

Norbert Steinfeldt

Tel.: +49 (0)381 1281 319

E-mail: norbert.steinfeldt@catalysis.de

Graphical abstract

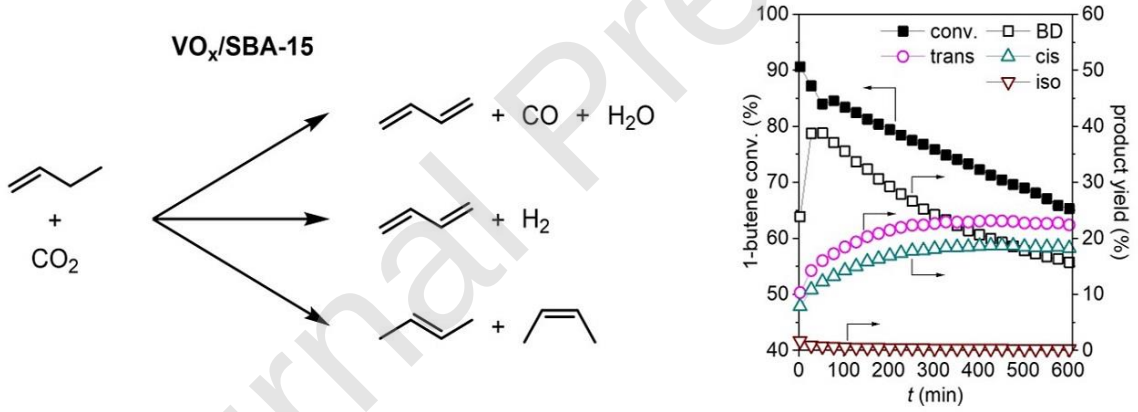

Highlights

- Butadiene (BD) can be formed from 1-butene on VO_x/SBA-15 in presence of CO_2
- maximum BD yield and selectivity of 39 % and 46 % were achieved
- CO_2 atmosphere has a positive effect on BD yield and coke formation

- VO_x single sites produced more BD per coke equivalent than polymerized or crystalline VO_x structures

Abstract

Butadiene (BD) is an important intermediate in chemical industry and is obtained predominantly from fossil sources. In the future new and sustainable BD sources and synthesis routes might be required to meet the rising demands for this compound. Here, the synthesis of BD from 1-butene in the presence of CO_2 was studied using supported vanadium oxide as active compound. Among the tested supports SBA-15 was shown to be the most effective one and a maximum BD yield of 39 % could be achieved. The VO_x/SBA-15 catalysts were characterized by complementary methods to obtain insight about the effect of catalyst synthesis and vanadium loadings on the formation of VO_x surface structures as well as the catalytic performance. CO_2 has a positive impact on the reaction. Coking was considered to be the main reason for the catalyst deactivation and the decreasing BD yield with increasing time on stream.

Keywords: butadiene, carbon dioxide, vanadium, 1-butene, dehydrogenation

1 Introduction

The climate change caused by the greenhouse gas CO_2 urges the industries around the world to scale down their vast CO_2 emissions and to develop processes which use this non-toxic gas for the production of valuable materials [1]. CO_2 has already been successfully applied as a soft oxidant in the dehydrogenation of light alkanes and ethyl benzene [2-9]. In contrast to other oxidants CO_2 does not over-oxidize the educt, its use inhibits the formation of hot spots, and lowers explosion risks. Moreover, it is usually reduced to CO which is a valuable C1 building block.

Butadiene (BD) is an important bulk chemical in the synthesis of elastomers and polymer resins [10]. Until now BD is predominantly extracted from refinery waste gas and natural gas condensates and the demand for BD is still expected to increase [11]. A more sustainable way of BD production would be the appropriate processing of biomass derived feedstocks like ethanol [12] and C4 alcohols [13]. The dehydration of

1-butanol, for example, yields butene that can be dehydrogenated to BD [14]. Another substance which is available from biomass is γ-valerolactone. It can be converted over acid catalysts with high selectivity to a mixture of butenes and CO_2 [15].

In general, two possible pathways for 1-butene dehydrogenation to BD with CO_2 are discussed: an oxidative and a non-oxidative one [16]. The oxidative dehydrogenation pathway (ODH) results in the formation of BD, water and CO (1). The non-oxidative dehydrogenation pathway (DH) leads to the formation of BD and molecular hydrogen (2). The dehydrogenation reactions can be affected by several side reactions: CO_2 can react with hydrogen that is formed during the reaction to form water and CO (RWGS) (3), 1-butene can isomerize to *cis*- or *trans*-butene (4), and polymerization of the olefins or adsorbed intermediates results in the formation of coke. Both dehydrogenation pathways are even at 873 K endergonic but the DH is thermodynamically slightly favored compared to the ODH. The Gibbs free energy of the RWGS at 873 K is relatively close to zero which indicates that the reaction can also proceed.

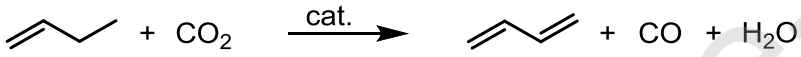

(1)

$\Delta_r G^0_m$ (873 K) = 19.2 kJ/mol

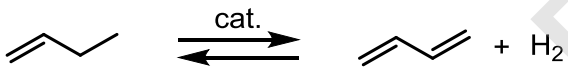

(2)

$\Delta_r G^0_m$ (873 K) = 12.5 kJ/mol

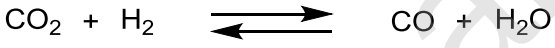

(3)

$\Delta_r G^0_m$ (873 K) = 6.7 kJ/mol

(4)

Most attention in the dehydrogenation of 1-butene with CO_2 was paid to Fe based systems [17-20] but Pt [21] and Cr [16] containing catalysts were also investigated. The catalytically active metal compound was either deposited on the surface of a carrier material or incorporated into the support. The materials with high specific surface areas and/or mesopores were favored since they can provide a high number of catalytic active sites. Well distributed active sites reveal a higher catalytic stability compared to Fe bulk phases [18, 22]. The presence of Lewis acid sites which could be

also provided by the support had also a positive impact on the BD formation [19, 20]. Furthermore, the catalysts should be able to activate CO_2 which was previously related to the oxygen mobility of the catalytic active compound [19]. In addition, the results in the dehydrogenation reactions of other light alkanes in presence of CO_2 using vanadia supported catalysts [23-26] encourage testing of those materials in the dehydrogenation of 1-butene in presence of CO_2. However, the features that determine the catalytic performance of VO_x surface species are still being debated [27]. The aim of the present work is to elucidate the effect of the support, V loading, VO_x structures, and selected reaction parameters on BD yield, production rate, selectivity as well as coke and side product formation.

2 Experimental

2.1 Catalyst preparation.

The syntheses of Al_2O_3, TiO_2 and ZrO_2 supports are described in the supplementary material (SM). SBA-15 was synthesized as follows: 25 g Pluronic® P123 (Sigma Aldrich) were poured into 600 g deionized water and 120 g HCl (37 %, Fisher Chemicals) while stirring at RT. When the solution became clear 48 g of tetraethyl orthosilicate (TEOS, 98 %, Alfa Aesar) were added. Within 1 h the mixture was heated up to 45 °C and stirred at this temperature for 24 h. Then, stirring stopped, and the suspension was kept at 90 °C for 3 days. Afterwards, the suspension was cooled down to RT and filtrated. The obtained solid was washed with 300 mL deionized water and dried (1 day at RT, additional 4 h at 90 °C). The dry solid was heated up to 550 °C within 10 h in a muffle furnace and kept at this temperature for 6 h. Finally, 13 g of SBA-15 were obtained.

Three different methods were applied to deposit VO_x species on the SBA-15 surface. Firstly, V_2O_5 (≥ 99 %, Merck) and oxalic acid (dihydrate, ≥ 99 %, Merck) were added to 30 mL deionized water. The amounts added were 20.7 mg V_2O_5 and 43.4 mg oxalic acid (Aq1.2), 42.5 mg and 88.3 mg (Aq2.4), or 89.4 mg and 185.8 mg (Aq5.4). The obtained suspension was heated up to 80 °C under stirring. After 30 min of stirring a clear blue solution was obtained which was cooled down to RT. Then, 800 mg of SBA-15 were added to the clear solution and the obtained suspension was stirred at RT for an additional 30 min. Afterwards, the solvent was evaporated under reduced pressure (temperature did not exceed 70 °C) and the residual solid was dried at 70 °C

for 16 h. Finally, the solid material was calcined in a tubular furnace at 600 °C for 5 h (heating rate 5 K/min) in an oxygen atmosphere (flow rate 20 mL/min). This method was also applied to deposit VO_x on Al_2O_3, ZrO_2, and TiO_2.

Another series of catalysts was prepared by impregnation of dried SBA-15 support with a solution of vanadium(V) triisopropoxide oxide (Alfa Aesar, 96 %). The impregnation was conducted inside of a glovebox using dry isopropanol as solvent. The catalysts were named Im2.4, Im3.7, and Im7.5. 1.000 g SBA-15 was impregnated with a solution of 0.126 mL V-precursor and 1.180 mL isopropanol (Im2.4), 0.266 mL and 1.040 mL (Im3.7), or 0.596 mL and 0.710 mL (Im7.5). Afterwards, the resulting materials were dried overnight under Ar flow in a Schlenk tube immersed in an oil bath heated up to 120 °C. The obtained powders were calcined as previously described.

For grafting of V on SBA-15, 2.0 g of dried vanadyl acetylacetonate (99 %, Acros) was poured into 800 mL of dry toluene. The suspension was stirred at RT under Ar overnight and then filtrated. 800 mg of dry SBA-15 were added to the filtrate and stirred at RT under Ar for 24 h. The suspension was centrifuged and the residue was washed 3 times with 80 mL toluene. Finally, the solid was dried at 80 °C overnight and calcined as described earlier. This catalyst was named Gr0.6.

2.2 Characterization.

The V amount was determined by ICP-OES analysis. 10 mg of catalyst were chemically digested in 8 mL aqua regia using a microwave (Multiwave PRO, Anton Paar). The obtained solution was filled up to 100 mL and measured in a Varian 715-ES ICP emission spectrometer.

An ASAP 2010 (Micromeritics) porosimeter was used to determine specific surface area and pore volume of the catalysts. Granulated samples (grain diameter 200–315 µm) were heated up to 200 °C at a pressure range of 1 – 10^{-2} mbar for 3 h. The isotherms were recorded using liquid nitrogen as adsorbate at a temperature of -196 °C. The Brunauer-Emmett-Teller (BET) method was used to calculate the specific surface areas. The pore volumes were obtained from the desorption branch of the sorption isotherm using the Barrett-Joyner-Halenda (BJH) method.

X-ray diffraction (XRD) powder patterns were recorded on a Panalytical X'Pert diffractometer equipped with a Xcelerator detector using automatic divergence slits and Cu Kα1 radiation (40 kV, 40 mA; λ = 0.15406 nm). The measurements were

performed in 0.0167° steps. The samples were mounted on silicon zero background holders. The obtained intensities were converted from automatic to fixed divergence slits (0.25°) for further analysis. Peak positions and profile were fitted with Pseudo-Voigt function using the HighScore Plus software package (Panalytical). Phase identification was done using the PDF-2 database of the International Center of Diffraction Data (ICDD).

Scanning transmission electron microscopy (STEM) measurements were performed at 200 kV with a probe aberration-corrected JEM-ARM200F (microscope: JEOL, Japan; corrector: CEOS, Germany) using annular bright field (ABF) and high angle annular dark field (HAADF) detectors. The microscope is equipped with a JED-2300 (JEOL) energy-dispersive x-ray-spectrometer (EDXS) for chemical analysis. The sample was deposed on a holey carbon supported Cu-grid (mesh 300) without any pretreatment and transferred to the microscope.

UV-Vis diffuse reflection spectra of dehydrated vanadia catalysts were recorded in diffuse reflectance mode at room temperature by an Ava Spec-2048 UV-Vis spectrometer (Avantes Inc., Apeldoorn, The Netherlands) equipped with a FCR-7UV400C-2ME optical probe (Avantes Inc., Apeldoorn, The Netherlands). $BaSO_4$ was used as white reference material. Each sample was placed in the middle of a quartz tube with an inner diameter of about 8 mm and fixed with quartz wool. Some of the samples were diluted with SBA-15. Each sample was dried under a synthetic air flow (total flow= 100 mL/min) at 350 °C for 2 h. After cooling to 25 °C both ends of the quartz tube were closed with plugs. Subsequently the UV-Vis spectrum was recorded at the position of the dried sample.

The differential thermal analysis (DTA) and differential scanning calorimetry (DSC) were performed by a Netzsch STA STA449 F3 Jupiter system (reference Al_2O_3) with a heating rate of 10 K/min from 25 °C to 800 °C. Nitrogen and synthetic air were used as carrier gases.

Temperature programmed reduction (TPR) was conducted with a BELCAT II (MicroBEL) equipped with a TCD detector. The samples (125-140 mg VO_x/SBA-15, 14 mg V_2O_5) were pretreated for 1 h at 600 °C in 30 mL/min synthetic air flow. After cooling them down to RT in air they were purged subsequently in 30 mL/min Ar flow for 30 min. For the measurement a gas mixture of 5 % hydrogen in Ar (total flow

30 mL/min) was applied and the samples were heated with a rate of 10 K/min from 25 to 1000 °C.

2.3 Catalytic tests.

200 mg of the catalyst (grain diameter 200–315 µm) were placed in a quartz tube (inner diameter 6 mm) that was installed in a furnace. Inside the reactor a second quartz tube (outer diameter 3 mm) equipped with a thermocouple was placed. The catalyst was heated up to 600 °C under a nitrogen flow (30 mL/min). When the reaction temperature was achieved the gas composition was changed from nitrogen to a mixture of 1-butene (3 mL/min), CO_2 (24 mL/min) and He as internal standard (3 mL/min). The gas mixtures were analyzed by gas chromatography (GC). The organic compounds were analyzed with a GC2010 (Shimadzu) equipped with a Select Al_2O_3 capillary column and flame ionization detector (FID). The permanent gases were analyzed in a GC2014 (Shimadzu) equipped with two packed columns (PoraPak Q, mole sieve), a thermal conductivity detector (TCD), a methanizer and a FID.

Conversions (conv.), yields, selectivities (sel.) and carbon balances (CB) were calculated from the chromatograms.

Conversion of 1-butene (CO_2 conversion was calculated in a similar manner, $\dot{n}$ is the flow rate in mmol/min)

$$\text{conv.} = \frac{\dot{n}_{1-\text{butene}}^{\text{inlet}} - \dot{n}_{1-\text{butene}}^{\text{outlet}}}{\dot{n}_{1-\text{butene}}^{\text{inlet}}} \cdot 100\% \quad (1)$$

Yield of alkane or alkene (i = C1 – C4, F_i is the number of carbon atoms in the molecule, e.g., $F_{C1} = 1$, $F_{1\text{-butene}} = 4$)

$$\text{yield}_i = \frac{\dot{n}_i^{\text{outlet}} \cdot F_i}{\dot{n}_{1-\text{butene}}^{\text{inlet}} \cdot F_{1-\text{butene}}} \cdot 100\% \quad (2)$$

Selectivity

$$\text{sel.} = \frac{\text{yield}}{\text{conv.}} \cdot 100\% \quad (3)$$

The carbon balance (CB)

$$CB = \frac{\sum_i \dot{n}_i^{outlet} \cdot F_i}{\dot{n}_{CO2}^{inlet} \cdot F_{CO2} + \dot{n}_{1-butene}^{inlet} \cdot F_{1-butene}} \cdot 100\% \quad (4)$$

The specific BD production rate (sBDP) describes the BD formation per time per mol V. M_V is the molar weight of V (50.94 g/mol) and x_V is the mass fraction of V in the catalyst.

$$sBDP = \frac{\dot{n}_{1-butene}^{inlet} \cdot yield_{BD} \cdot M_V}{m_{cat} \cdot x_v} \quad (5)$$

The V surface density (SD) was calculated using the Avogadro constant N_A and the specific surface area obtained from BET measurements (SSA).

$$SD = \frac{x_V \cdot N_A}{M_V \cdot SSA} \quad (6)$$

3 Results

3.1 Catalytic results

3.1.1 Influence of the support material

Firstly, different metal oxide supports (SiO_2, Al_2O_3, ZrO_2 and TiO_2) were loaded with VO_x (nominal V loading = 1.2 wt-%) and tested in the dehydrogenation reaction. The BET surface area of the VO_x/MO_x catalysts ranged between 24 and 690 m^2/g (Tab. S1). Only SiO_2 supported VO_x (Aq1.2) showed weak reflections of V_2O_5 but this was not the case for the other prepared catalysts (Fig. S1, Fig. 8A). As presented in Fig. 1A all catalysts revealed a relatively high initial 1-butene conversion which peaked between 73 and 84 %. VO_x/ZrO_2 and VO_x/TiO_2 catalysts showed a decline in 1-butene conversion of over 60 % within the first 30 min of time-on-stream (TOS). In case of VO_x/Al_2O_3 1-butene conversion decreased from 84 to 28 % within 5 h. The slowest decline in 1-butene conversion was observed for VO_x/SBA-15 (Aq1.2) where conversion decreased only slightly from 84 to 75 % within 10 h. As shown in Fig. 1B, the VO_x/SBA-15 revealed also the highest initial BD selectivity among all studied catalysts (38 %) which, however, continuously dropped with increasing TOS. The initial BD selectivity of VO_x/Al_2O_3 was the lowest (14 %) but increased with increasing TOS to about 36 %. The highest BD yield was obtained with VO_x/SBA-15 (Fig. 1C). Here, the BD yield decreased within 10 h from 32 to 15 %. The BD yield of VO_x/Al_2O_3 increased within the first 50 min of TOS to the same value as obtained with VO_x/SBA-

15 (24 %) but a much faster decline in 1-butene yield with increasing TOS was observed compared to VO_x/SBA-15. ZrO_2 and TiO_2 supported vanadia catalysts showed an initial BD yield of 24 and 20 %, respectively, which dropped sharply within 30 min to values below 4 %. Because the VO_x/SBA-15 catalyst showed the highest 1-butene conversion and BD yield this kind of material was chosen for further studies.

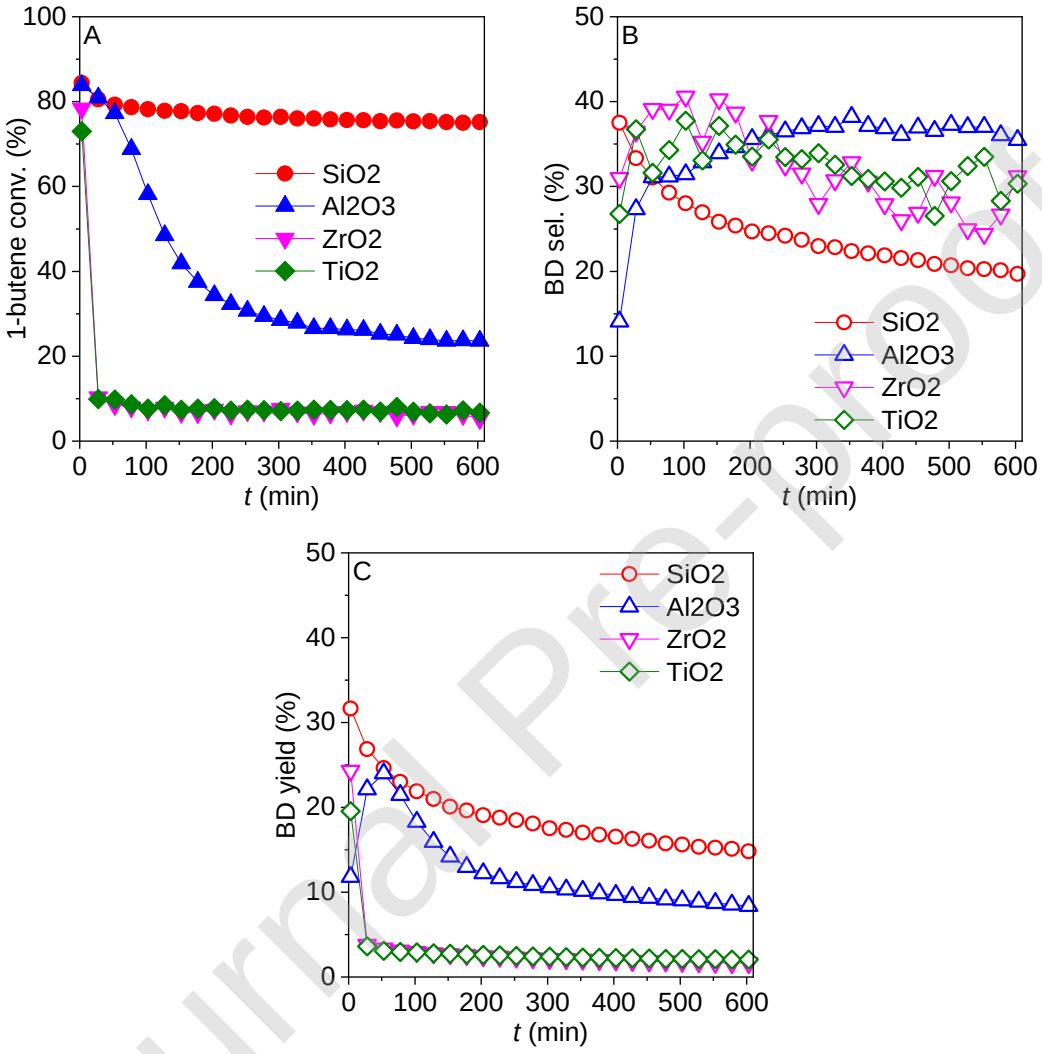

Fig. 1. A) 1-Butene conversion, B) BD selectivity and C) BD yield versus time on stream using different VO_x/MO catalysts (nominal V loading = 1.2 wt%). Conditions: 200 mg catalyst, 3 mL/min 1-butene, 3 mL/min He, 24 mL/min CO_2, T = 600 °C, p = 1.15 bar.

3.1.3 VO_x/SBA-15 catalysts with different V loading

The catalytic performance of the different VO_x/SBA-15 catalysts is presented in Fig. 2. Catalysts prepared in aqueous solution (Aq series) showed only relatively small differences in their performance (Fig. 2A). 1-butene conversion decreased within 10 h from about 85 to 75 % while the BD selectivity dropped from approximately 37 to about

21 %. A maximum BD yield of 32 % was achieved at the beginning of the reaction (Fig. 2C). The catalytic stability of these materials was slightly improved when the V loading increased from 1.2 to 2.4 wt-%. A further increase in V content (up to 5.3 wt-%) did not affect the catalytic performance. The catalyst prepared by grafting (Gr0.6) showed a similar catalytic performance to that of the catalysts of the Aq series despite its lower V content.

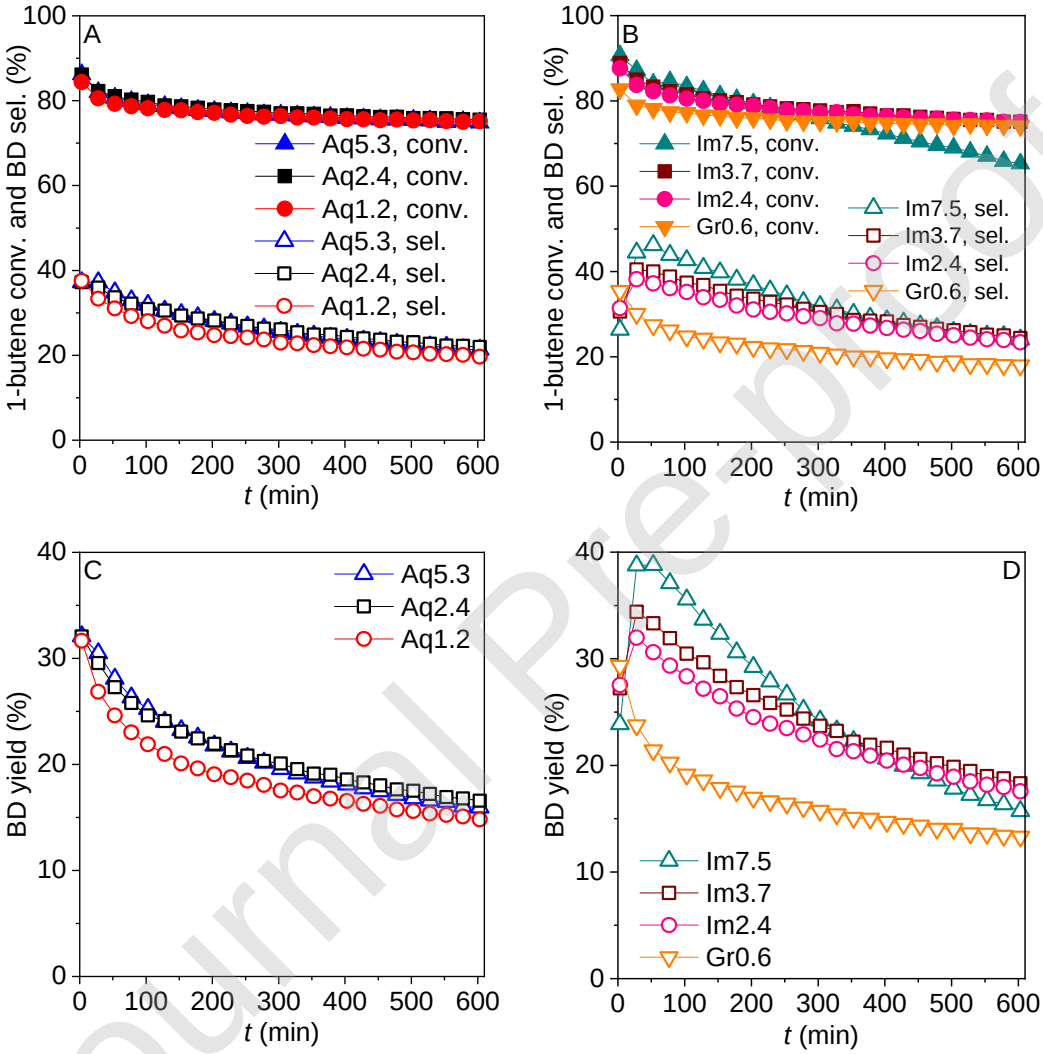

Fig. 2. 1-Butene conversion, BD selectivity (A, B) and BD yield (C, D) versus time on stream for different VO_x/SBA-15 catalysts. Conditions: 200 mg catalyst, 3 mL/min 1-butene, 3 mL/min He, 24 mL/min CO_2, T = 600 °C, p = 1.15 bar.

For the catalysts impregnated using isopropanol (Im series) the initial 1-butene conversion increased with increasing V loading (Fig. 2B). Moreover, BD selectivity and yield achieved their maximum between 28 and 53 min TOS before declining continuously (Fig. 2B and D). With catalyst Im7.5 a maximum BD yield of 39 % and a

maximum BD selectivity of 46 % were achieved. Noticeably, this catalyst exhibited also the strongest deactivation among all studied catalysts. 1-butene conversions, BD selectivities and BD yields of all seven catalysts are also compared at 53 and 153 min TOS in Fig. S7. In general, for conversion, selectivity and yield the following trend can be observed: Gr0.6 < Aq series < Im series. Within the Im series all three values increase with increasing vanadium loading. The trend is less pronounced in the Aq series.

The temporal evolution of *trans*-, *cis*-, and *iso*-butene is shown in Fig. 3A for Aq2.4 and in Fig. 3B for Im7.5. At the beginning of the reaction the BD yield on both catalysts was clearly higher than those of *cis*- and *trans*-butenes. With increasing TOS, BD yield decreased and that of 2-butenes increased. At longer TOS, the latter became the main products. The isomerization of 1-butene to 2-butenes was also the main reaction when using pure SBA-15 as the catalyst (Fig. S2). *Iso*-butene was formed only in low amounts (< 2 %) on both catalysts.

Fig. 3C and D show the influence of TOS on CO, hydrogen and BD formation. The highest amounts of CO and hydrogen were always detected directly at the beginning of the reaction and the amount of CO was higher than that of hydrogen and BD. CO and hydrogen formation was stronger on Im7.5 than on Aq2.4. With increasing TOS, CO and hydrogen amounts decreased on both catalysts and CO achieved a similar flow rate like BD. It is worth noting that Aq2.4 was also tested in the RWGS reaction (Fig. S8). As shown, hydrogen and CO_2 were consumed to form CO and water. The evolution of minor organic side products (C1-C4) is depicted in Fig. S4C for Aq2.4 and in Fig. S5C for Im7.5. Initial yields of C1-C3 cracking products are higher on Im7.5 than on Aq2.4.

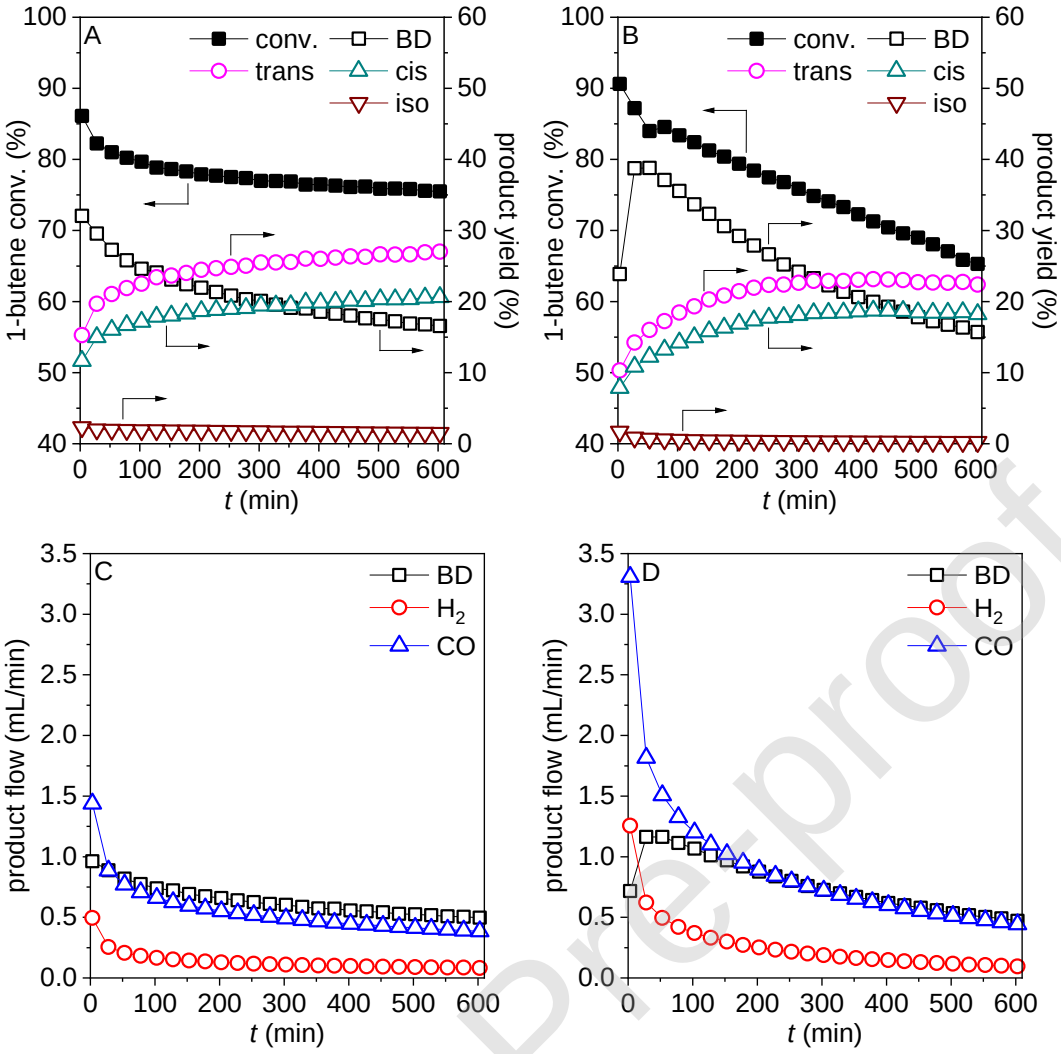

Fig. 3. 1-Butene conversion and yields of BD, *trans*-butene, *cis*-butene and *iso*-butene using A) Aq2.4 and B) Im7.5. Flow of BD, H_2 and CO using C) Aq2.4 and D) Im7.5. Conditions: 200 mg catalyst, 3 mL/min 1-butene, 3 mL/min He, 24 mL/min CO_2, T = 600 °C, p = 1.15 bar.

Fig. 4 shows the temporal evolution of the carbon balance (CB). The CB was calculated from the flow rates of C1-C4 products leaving the reactor (see equation 4). CB values lower than 100% are assumed to be caused by carbon species that stay inside the reactor, mainly on the catalyst surface, as coke. In general, coke formation is strongest directly at the beginning of the reaction and decreases with increasing TOS to a constant value (Fig. 4A and B). For coke formation within 120 min TOS the following order was observed: Im series > Aq series > Gr0.6. Moreover, within the Im series, coke amount increases with increasing vanadium loading. In case of the Aq series this trend was less pronounced.

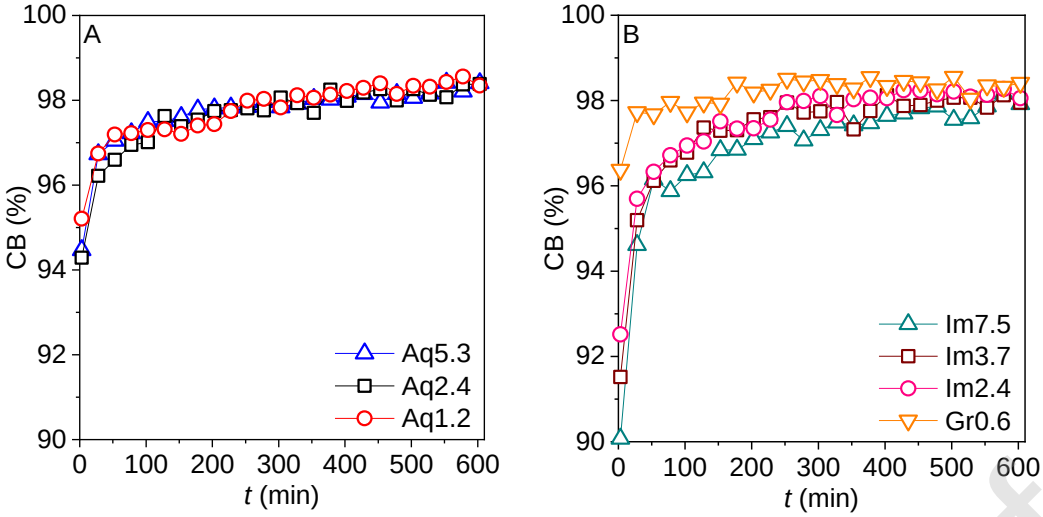

Fig. 4. Carbon balance versus time on stream for the different catalysts. Conditions: 200 mg catalyst, 3 mL/min 1-butene, 3 mL/min He, 24 mL/min CO_2, T = 600 °C, p = 1.15 bar.

Fig. 5 compares the CO_2 conversion of all VO_x/SBA-15 catalysts which was expected to be lower than the 1-butene conversion due to the large excess of CO_2 in the reaction feed. In general, CO_2 conversion increased with increasing V loading. Differences in CO_2 conversion for the various V loadings were more significant for the Im series than for the Aq series. Moreover, CO_2 conversion obtained with the catalysts of the Im series at comparable V loadings was higher than those of the Aq series. Using Im7.5, up to 11 % of CO_2 was initially converted. Within 10 h CO_2 conversion dropped continuously reaching a final value between 1 and 3 %.

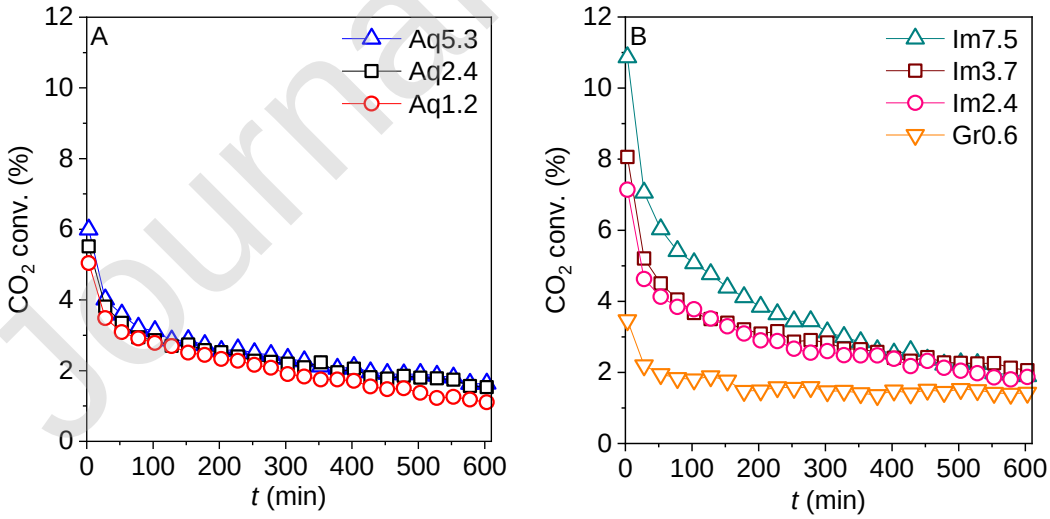

Fig. 5. CO_2 conversion of different catalysts versus time on stream. Conditions: 200 mg catalyst, 3 mL/min 1-butene, 3 mL/min He, 24 mL/min CO_2, *T* = 600 °C, *p* = 1.15 bar.

3.1.4 Influence of selected reaction parameters

Catalyst Aq2.4 was chosen to study the effect of water addition, nitrogen atmosphere, reaction temperature, and hydrogen pre-treatment on 1-butene conversion and BD yield (Fig. 6). When water was introduced as steam into the feed (Fig. 6A) both 1-butene conversion and BD yield decreased compared to the experiment without steam addition but the drop of conversion and yield with increasing TOS proceeded in both feed compositions at a similar rate. Fig. S3 compares the formation of CO and hydrogen as well as the selectivity of 2-butenes of the experiments with and without steam addition. When the educt feed contained water, the amount of CO formed was significantly lowered while slightly more hydrogen was produced. The selectivity of 2-butenes was higher when steam was added.

When the reaction was performed in nitrogen instead of CO_2 the 1-butene conversion was slightly higher, however, the BD yield decreased significantly (Fig. 6B). Furthermore, the yields of *iso*-butene (Fig. S4A and B) as well as of propene, ethene and methane (Fig. S4C and D) were significantly increased. Moreover, the amount of hydrogen was 3 - 4 times higher in nitrogen than in CO_2 atmosphere and only traces of CO were detected (Fig. S4E and F).

With increasing reaction temperature from 575 °C to 620 °C both 1-butene conversion and BD yield increased (Fig. 6C). A similar behavior was recently observed for the Cr-SiO_2 catalyst and explained by the fact that higher temperatures favor the dehydrogenation reaction compared to isomerization [16].

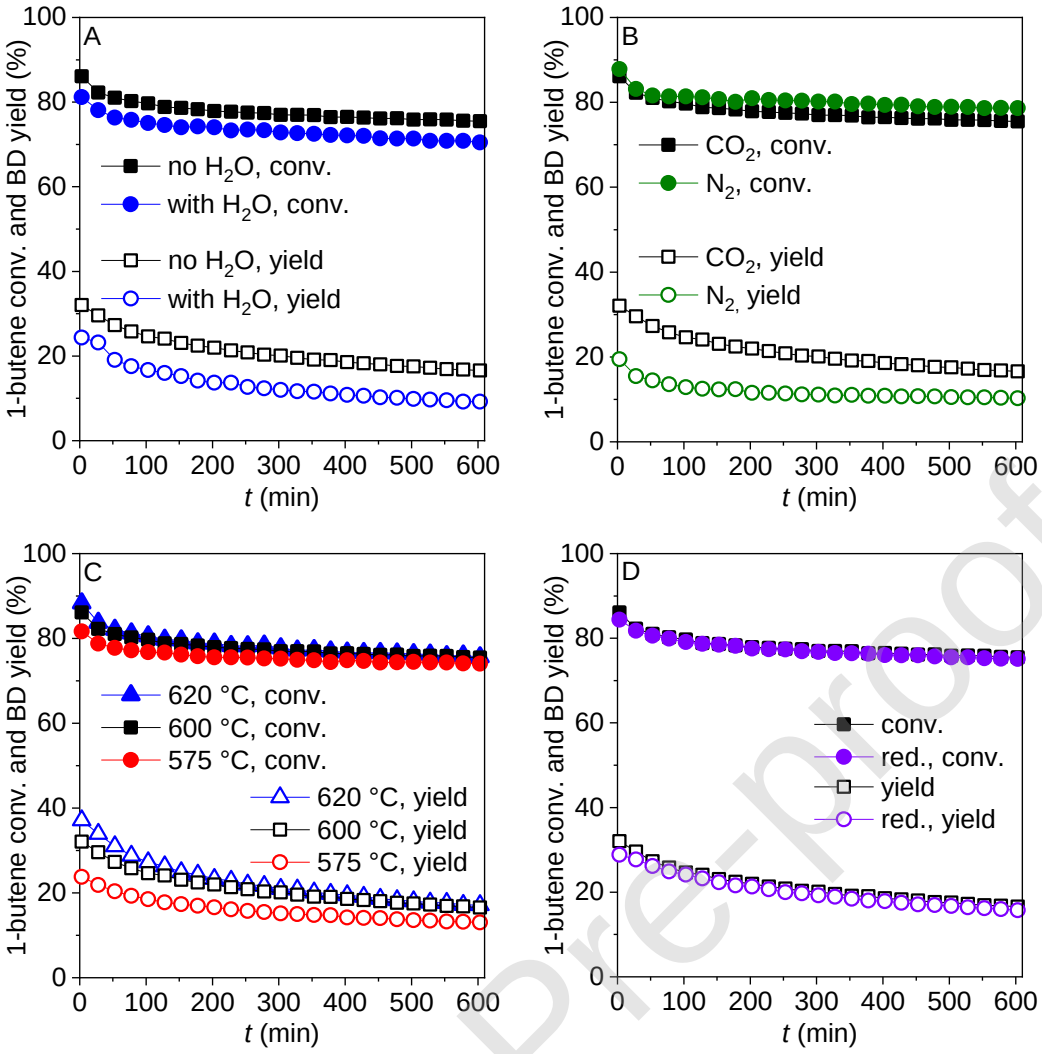

Fig. 6. Influence of selected reaction parameters on 1-butene conversion and BD yield using Aq2.4; A) 3 mL/min H_2O steam were introduced in the educt flow, B) CO_2 was replaced with N_2, C) influence of reaction temperature, D) the catalyst was pre-reduced for 90 min at 600 °C with a mixture of 6 mL/min H_2 and 30 mL/min N_2 before the educt flow was introduced. Conditions: 200 mg catalyst, 3 mL/min 1-butene, 3 mL/min He, 24 mL/min CO_2 (21 mL/min CO_2 in case of A, 24 mL/min N_2 in case of B).

The hydrogen pretreatment had almost no effect on 1-butene conversion and BD yield of Aq2.4 as shown in Fig. 6D. Differences in the as-prepared and pre-reduced catalyst were observed in the case of Im7.5 (Fig. S5). The reduced catalyst showed a slightly lower initial 1-butene (3 %) (Fig. S5A, B) and CO_2 (3 %) conversion (Fig. S6A), however, initial BD yield increased from 24 to 35 % (Fig. S5A, B). Moreover, the initial CB was also improved when the catalyst was pre-reduced (Fig. S6B). Both the reduced and unreduced catalysts achieved their maximum BD yield within 53 min. Between 53 min and 350 min of TOS the BD yield was slightly higher on the unreduced catalyst than on the pre-reduced one. Furthermore, the pre-reduction decreased both the initial

amounts of organic cracking products (Fig. S5C and D) and of CO and hydrogen (Fig. S5E and F).

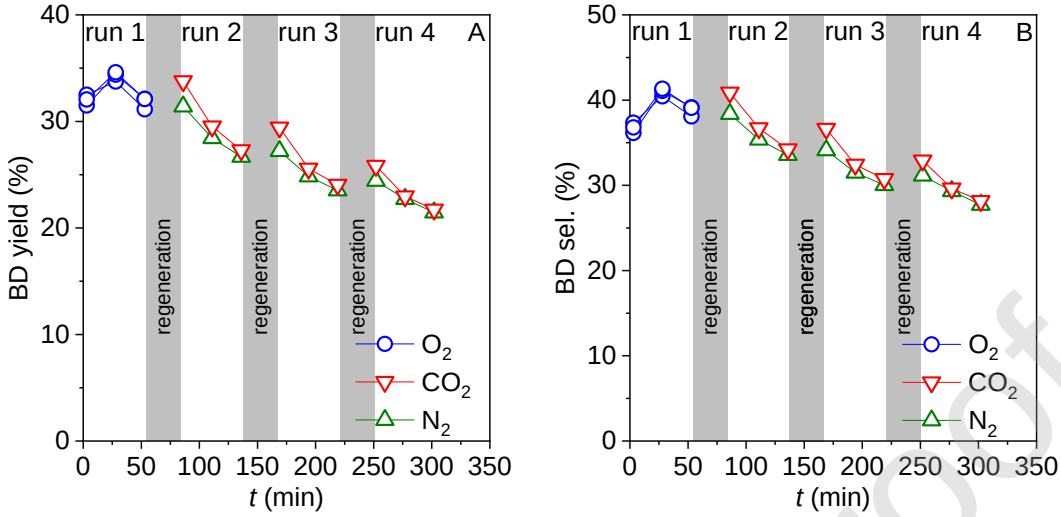

Fig. 7. A) BD yield and B) BD selectivity in a regeneration experiment testing Im2.4. Prior to the first runs the catalyst was regenerated at 600 °C for 30 min with 15 mL/min synthetic air + 15 mL/min N_2 and purged for 10 min with 30 mL/min N_2. Prior the 2nd, 3rd and 4th run the catalyst was pre-treated with 24 mL/min CO_2 + 3 mL/min He or with 30 mL/min N_2 for 30 min (Conditions: 200 mg catalyst, 3 mL/min 1-butene, 3 mL/min He, 24 mL/min CO_2, T = 600 °C, p = 1.15 bar).

Finally, periodic switch experiments were performed to study the effect of different regeneration methods on the catalytic performance (Fig. 7). Therefore, used Im2.4 was re-oxidized inside the reactor using a mixture of air and nitrogen. Afterwards, the 1-butene/CO_2 feed was introduced (first run). As shown, BD yield and selectivity reach their maximum at 23 min (see also Fig. 2). At the end of the first run BD yield and selectivity were about 32 and 39%, respectively. At this stage it is assumed that vanadium sites were already partly reduced and that parts of the catalyst surface were covered by coke.

When the catalyst was regenerated with CO_2 for 30 min, initial BD yield and selectivity in the second run were higher (34 and 41%) than at the end of the first run. With increasing TOS, BD yield and selectivity dropped continuously. After the second regeneration with CO_2 (third run), the initial BD yield and selectivity increased again compared to the last value of the previous run, but with increasing TOS both BD yield and selectivity dropped again. The same trend was observed for the fourth run. As expected, a regeneration of the catalyst with CO_2 cannot stop the deactivation. The increase in initial BD yield and selectivity after pre-treatment with CO_2 might be

attributed to a partial oxidation of reduced vanadium species and/or the removal of carbon species from the catalyst surface by reaction with CO_2 [28]. When using nitrogen for regeneration, the increase in initial BD yield and selectivity was significantly lower compared to those with CO_2 but the drop in BD yield and selectivity with increasing reaction time was comparable.

3.2 Characterization of the as-prepared catalysts

XRD powder patterns of the fresh catalysts are presented in Fig. 8A. The pattern of pure SBA-15 showed a broad peak at $2\theta = 22°$ that is assigned to the amorphous silica structure [29]. The samples Aq1.2, Aq2.4, and Aq5.3 reveal additionally reflections of an orthorhombic V_2O_5 phase (PDF 00-041-1426) whose intensity increased with rising V loading. The size of the V_2O_5 crystallites calculated from the diffraction patterns using the Scherrer equation ranged between 37 and 52 nm. STEM images of Aq2.4 showed the coexistence of ordered and disordered SBA-15 domains (Fig. 9A) and confirm the existence of crystalline vanadia particles which were located outside of the channels of the SBA-15 support (Fig. 9B). Moreover, HAADF-STEM indicates the presence of thin non-crystalline polymeric VO_x species on the SiO_2 surface (Fig. 9D). The catalysts of the Im series showed beside the reflection at $2\theta = 22°$ additional broad peaks at 26.1° and 50.5° whose intensity increased with increasing vanadia loading. These reflections cannot be assigned to a known VO_x phase.

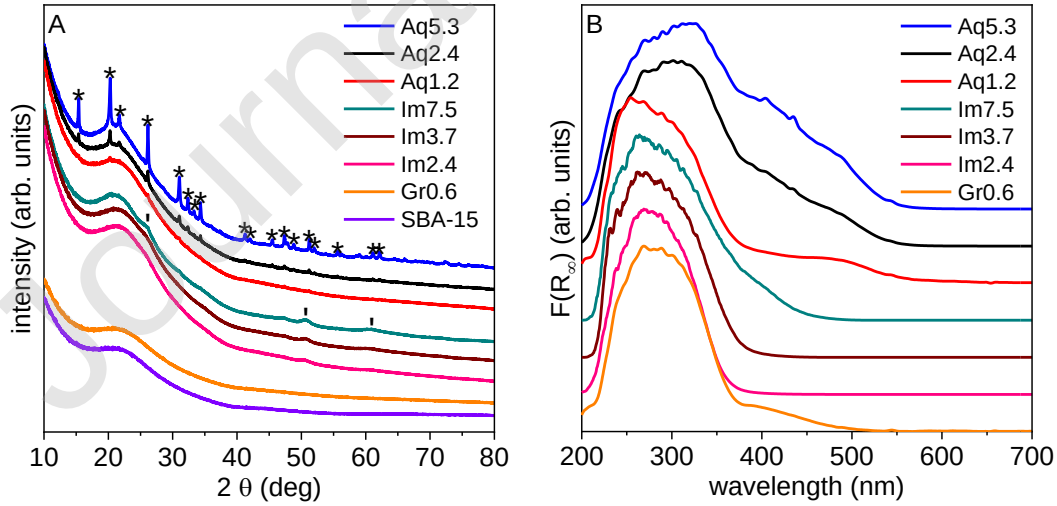

Fig. 8. A) XRD powder patterns of the as-prepared VO_x/SBA-15 catalysts, * indicates orthorhombic V_2O_5, B) normalized UV-Vis diffuse reflectance spectra of different catalysts (catalysts were dried in N_2 flow before measurement).

UV-Vis diffuse reflectance spectra of the dried catalysts are shown in Fig. 8B. Bands located between 250-300 nm were assigned to charge transfer transitions of tetrahedrally coordinated VO_x monomers [30]. Absorption around 350 nm is caused by VO_x tetrahedra which are linked in a chain like manner [30]. V_2O_5 absorbs at wavelengths above 400 nm [30]. Gr0.6 and the catalysts of the Im series showed independent of their V loading an absorption maximum below 300 nm. Im7.5 had additionally some light absorption around 400 nm. For the catalysts of the Aq series the absorption maxima vary with increasing V loading between 300 nm (Aq1.2) and 320 nm (Aq5.3) which might be caused by the presence of crystalline V_2O_5 structures on these catalysts. The percentages of VO_x single sites on the surfaces of the catalysts were assessed by the method of Gao *et al.* [31] and results are listed in Tab. 1. The Gr0.6 sample prepared by grafting contained nearly exclusively VO_x single sites. Samples prepared by incipient wetness impregnation using isopropanol as solvent (Im series) possessed at similar V loadings a higher amount of VO_x single sites than the samples of the Aq series. Because the catalysts of the Aq series contained additionally crystalline V_2O_5 particles the percentage of single sites determined by UV-Vis spectroscopy is less exact [32]. Generally, the population of single sites decreased with increasing V loading for both series and those of polymeric VO_x units and even V_2O_5 increased indicated by the bathochromic shift in light absorption.

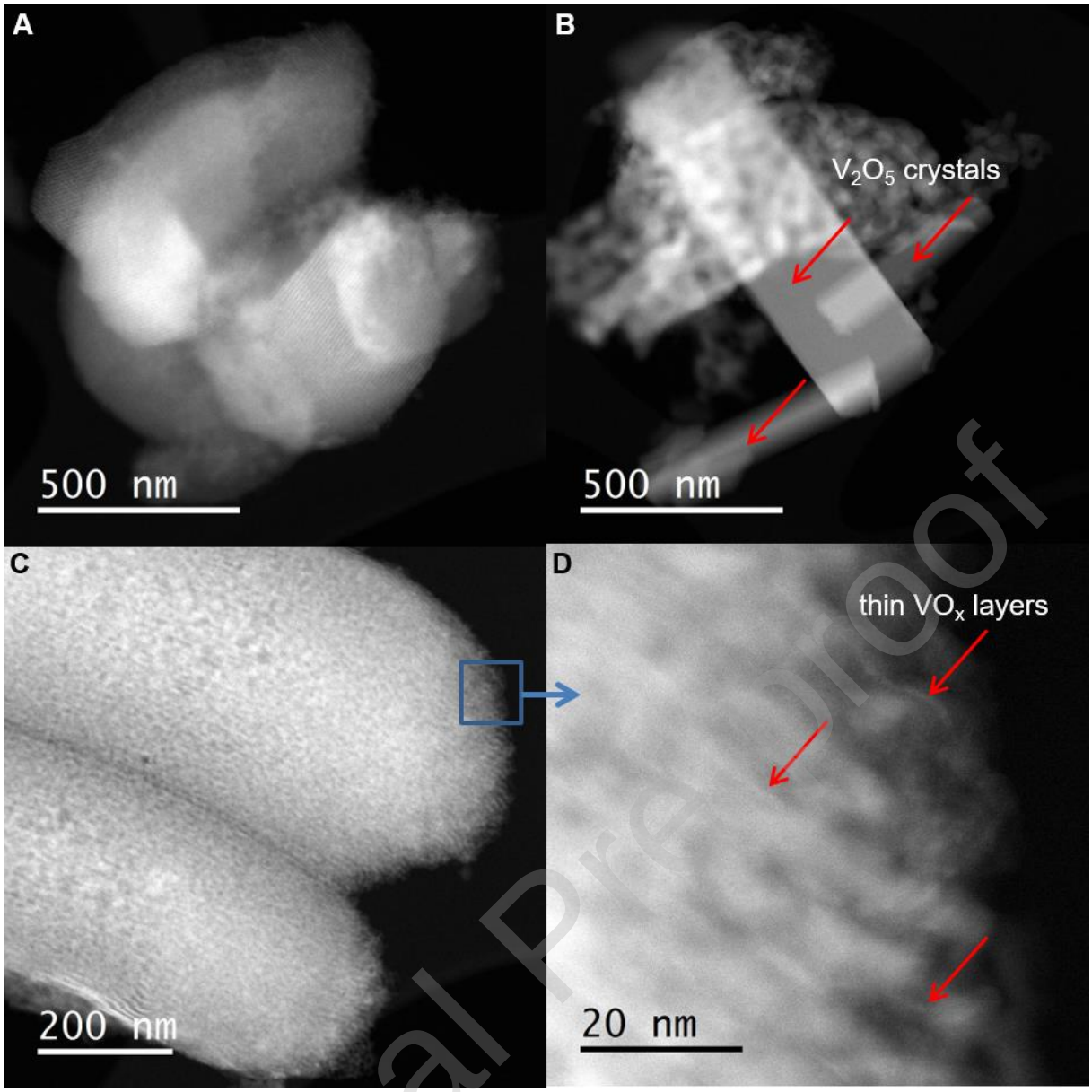

Fig. 9. HAADF-STEM images of catalyst Aq2.4 showing A) ordered and disordered structures of the support; B) the presence of relatively large vanadia crystals; C) a catalyst particle that possesses D) polymeric non-crystalline VOx domains.

Nitrogen adsorption and desorption isotherms are presented in Fig. S9A and B. All isotherms can be described as type IV which is typical for a mesoporous material [33]. The pore size distribution derived from the desorption branch of the isotherms are presented in Fig. S9C and D. Textural parameters derived from N_2-sorption experiments by BET and BJH methods are listed in Tab. 1. The specific surface area (SSA) and pore volume (V_p) are influenced by the V loading. The sample Gr0.6 which was prepared by grafting possessed the lowest V amount and exhibited the largest SSA (700 m^2/g) and highest V_p (0.98 mL/g) among all V containing catalysts. In general, BET surface area, pore volume, and mean pore diameter decreases with

increasing V loading. BET surface areas and pore volumes of Aq catalysts are higher than those of the Im catalysts. As shown by XRD and TEM a certain fraction of the VO_x species was here located outside of the SBA-15 particles reducing the vanadium amount deposited on the SBA-15 channel surface. SAXS patterns of fresh catalysts are presented in Fig. S10A and C. Peak maximum of SBA-15 d_{100} reflection ($2\pi/q$) was located at 9.44±0.03 nm (exception Im7.5: 9.3 nm). The mean wall thickness calculated by subtracting the mean pore diameter determined by the BJH method from the dimension of the unit cell ($a_0 = 2d_{100}/3^{1/2}$) was slightly higher for samples of the Im series (5 nm) than for the samples of the Aq series (4.6 nm, pure SBA-15: 4.3 nm). In accordance with the BET results (lower BET surface area and pore volume) this indicates a higher V loading in the channels of the Im series.

Tab. 1
General characteristics of the fresh catalysts.

Catalyst	V (wt-%)[a)]	SSA (m^2/g)[b)]	V_p (mL/g)[b)]	X_{mono} (%)	H_2 uptake (mmol/g)[d)]	av. ox. state[e)]
SBA-15	-	789[c)]	1.14[c)]	-	-	-
Gr0.6	0.6	700	0.98	97	0.083	3.59
Im2.4	2.4	601	0.80	72	0.457	3.05
Im3.7	3.7	559	0.78	45	0.716	3.03
Im7.5	7.5	364	0.64	2	1.437	3.04
Aq1.2	1.2	690	0.98	77[f]	0.202	3.28
Aq2.4	2.4	628	0.97	42[f]	0.461	3.05
Aq5.3	5.3	528	0.78	-[f]	1.066	2.95

a) data obtained from ICP; b) granulated material; c) powder; d) obtained from TPR; e) average V oxidation state after TPR, calculated from H_2 uptake; f) calculated despite presence of V_2O_5

The TPR profiles of the different catalyst are presented in Fig. 10. The shape of the TPR profile is strongly affected by the synthesis method while the intensity of the TPR signal and the position of the peak maximum depend on the V loading. The TPR profiles of Gr0.6 and those of the Im series showed only one approximately symmetric reduction peak whose intensity increases with increasing V loading. The Gr0.6 catalyst possesses a maximum which occurs at 545 °C (Fig. 10A). The peak maxima Im3.7 and Im7.5 shifted with increasing V loading to 585 °C and 600 °C, respectively compared to the 578 °C of Im2.4. This temperature shift might be caused either due to

the rising polymerization degree of the VO_x species [34, 35] as already indicated by the presented UV-Vis results or by a decreasing reduction rate with increasing V loading [35].

The TPR profiles of the Aq series showed either two maxima or a broad peak with a shoulder. Aq1.2 showed maxima at 564 °C and 631 °C while Aq2.4 at 571 °C and 666 °C (Fig. 10B). The profile of Aq5.3 exhibited besides the maximum at 645 °C a shoulder at about 580 °C. The first maxima of Aq1.2 and Aq2.4 and the shoulder of Aq5.3 are in the same temperature range as the maxima of the Im series, thus, they might be also attributed to the reduction of isolated and polymeric VO_x species. The maxima at higher temperatures (above 630 °C) might be assigned to the reduction of more bulky vanadium oxide species [23] which were identified by XRD (Fig. 8A). For comparison TPR profiles of V_2O_5 bulk phase was also recorded. As shown, the reduction of unsupported V_2O_5 only starts at about 600 °C and its TPR profile possesses several maxima [36]. They occur at higher temperatures than those observed in the as-prepared catalysts. The differences in the TPR profiles between the pure bulk V_2O_5 and the Aq catalysts indicate that the supported nanosized V_2O_5 particles are much easier to reduce than bulk V_2O_5 phases.

The hydrogen consumption of the single catalysts is presented in Tab. 1. For most catalysts the consumed hydrogen amount corresponds to a reduction of V(V) to V(III) (assumption: 1mol H_2 reduces 1 mol V_2O_5 to 1 mol V_2O_3). The larger deviation in case of Gr0.6 is assumed to be caused by the low V content of this sample.

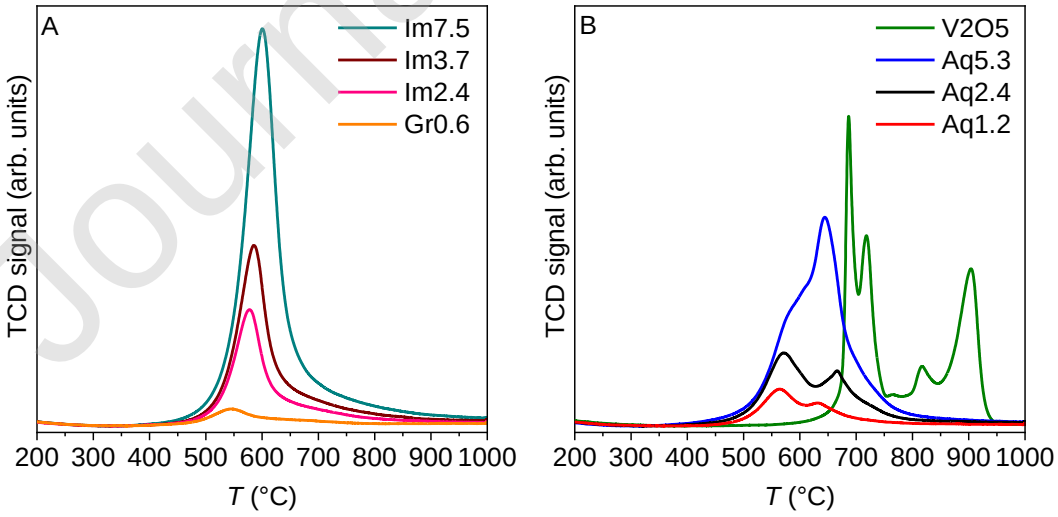

Fig. 10. TPR of A) Gr0.6, Im2.4, Im3.7, Im7.5 and B) Aq1.2, Aq2.4, Aq5.3 and V_2O_5. The signals of all VO_x/SBA-15 catalysts were normalized to the sample mass.

3.3 Characterization of the used catalysts

Comparison of the SAXS profiles of selected fresh and used catalysts showed that the dehydrogenation reaction had no effect on the SBA-15 structure (Fig. S10B and D). XRD powder patterns of the fresh and used Aq5.3 and Im7.5 catalysts are displayed in Fig. 11. While fresh Aq5.3 showed distinct reflections of a V_2O_5 phase, the used sample revealed exclusively reflections of a rhombohedral V_2O_3 phase (PDF 00-034-0187) with relatively low intensity. In contrast to Aq5.3, neither the fresh Im7.5 nor the used catalyst showed XRD reflexes of a known vanadium oxide phase. The weak, broad peaks at 2θ = 26.1° and 50.6° visible in the fresh sample disappeared in the used catalyst. Here, only a very broad unknown reflection at 2θ = 43.2° was detected.

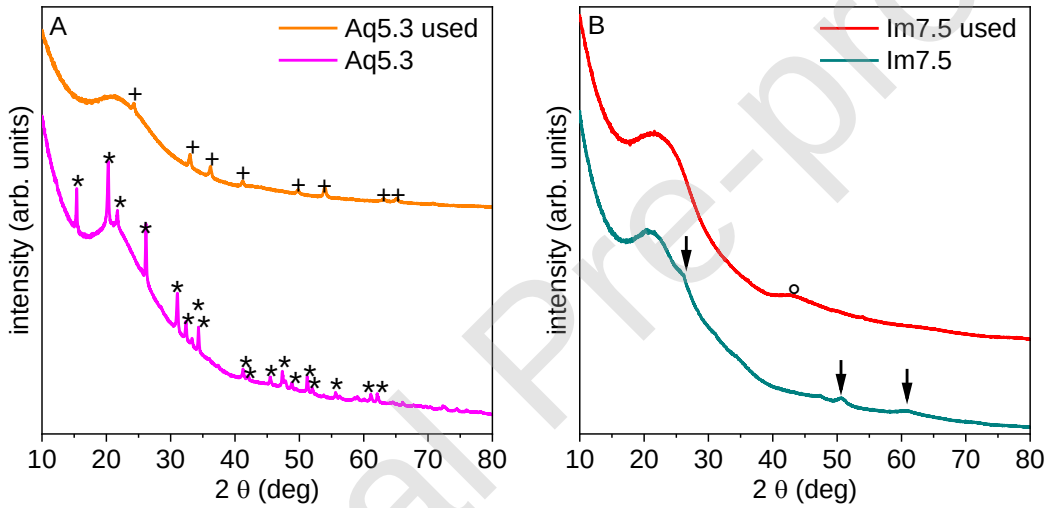

Fig. 11. A) XRD powder patterns of the fresh and used catalysts A) Aq5.3 (* indicates orthorhombic V_2O_5, + indicates reflections of a V_2O_3 phase) and B) Im7.5., signals denoted with ↓ and ° could not be assigned to any VO_x structures.

STEM images of a used Aq2.4 catalyst are presented in Fig. 12. The images show coke deposits which were located both on the silica surface and on the surface of the VO_x species. Interestingly, the images of the used catalyst also show small VO_x particles with distinct lattice planes which are not observed on the fresh catalyst (Fig. 12C, Fig. S11). This indicates a rearrangement of the VO_x species during the reaction. Coke deposition was further confirmed by EDX (Fig. S12 and 13). Results from XPS indicate lower atomic Si/C and V/C ratios in used catalysts than in the fresh ones (Tab. S2). Moreover, the C1s XP spectrum of the used catalyst Im7.5 shows the presence of coke and oxygen containing carbon species (Fig. S14) [37]. BET

measurements of a used Aq2.4 catalyst reveal a decline in surface area of 140 m^2/g and pore volume of 0.18 mL/g compared to the fresh catalyst which is assumed to be caused by blocking of channels through coke formation.

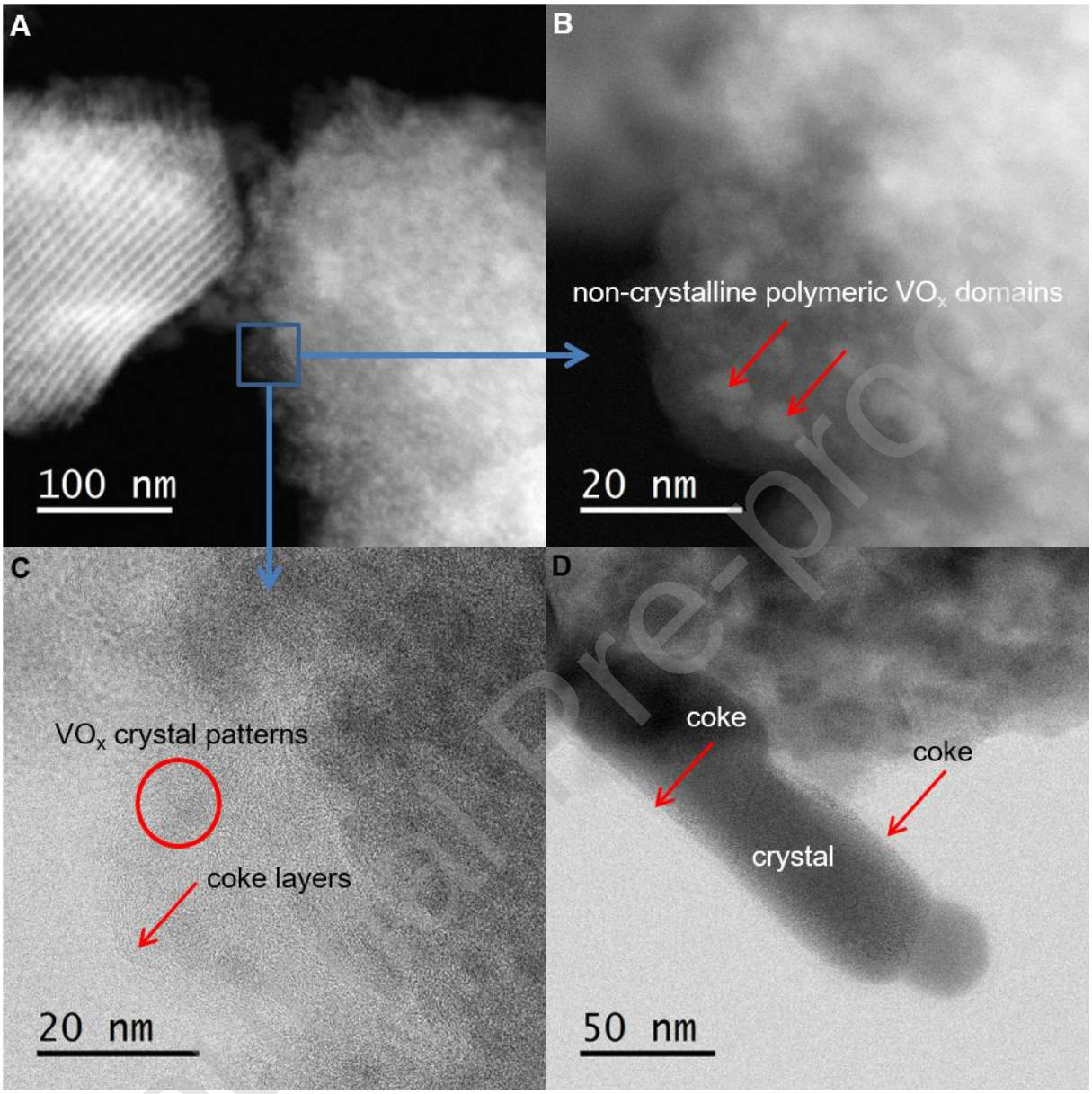

Fig. 12. HAADF-STEM images (A, B) and ABF-STEM images (C, D) of used Aq2.4 showing A) ordered and disordered structures of the SBA-15 support; B) non-crystalline polymeric VO_x; C) graphite type carbon layers and distinct patterns of small VO_x crystallites; D) VO_x crystals covered with coke.

Fig. 13A shows a plot of coke amount versus BD amount obtained after 10 h TOS for the different catalysts. The amount of coke deposits increases with increasing amount of BD formed. When CO_2 is replaced by nitrogen coking is much stronger while less BD is produced. In Fig. 13B the ratio m_{BD}/m_{coke} is plotted versus the V surface density (SD). For the catalysts of the Im series this ratio seems to be independent of the SD.

Higher values of this ratio were obtained for the Aq series. Here, this value decreased with decreasing number of isolated vanadium surface sites. Gr0.6 which has nearly only isolated VO_x single sites reveals by far the highest m_{BD}/m_{coke} ratio. The figures indicate that coke formation depends on BD formation and both are affected by the structure of the catalytic active vanadium site.

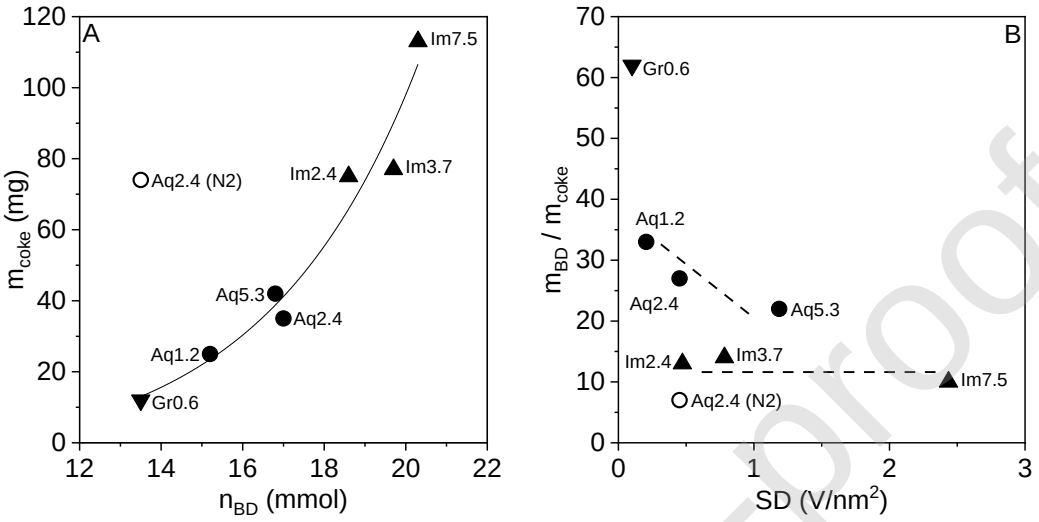

Fig. 13. A) plot of m_{coke} versus n_{BD} produced during 10 h TOS. The BD amount was calculated from GC measurements while the coke amount was derived from TGA measurements of the used catalysts. B) plot of m_{BD}/m_{coke} versus V surface density (SD).

3.4 Discussion

The structure of VO_x species on SBA-15 is affected by the applied synthesis method. Samples of the Aq series contained isolated VO_x units, two-dimensional VO_x domains and nanosized crystalline V_2O_5. The formation of the crystalline V_2O_5 phase can be explained as follows: A certain amount of the V precursor dissolved in water could not enter the SBA-15 channels because the precursor species agglomerated or precipitated outside of the SBA-15 channels. Thus, a bulk phase outside of the channels was formed and the final calcination converted this phase into nanosized crystalline V_2O_5 which was detected by XRD and STEM (Fig. 8A, Fig. 9). The amount of the VO_x phase outside of the channels depends on the concentration of the V precursor in the aqueous solution. In case of the Im catalysts, the V precursor could completely enter the channels which lead to a better V distribution. After calcination V(V) was obtained independent of the particular VO_x structure. This assumption is supported by TPR results where the measured hydrogen consumption corresponds approximately to a reduction of V(V) to V(III) (Tab. 1) [35].

When the fresh VO_x/SBA-15 catalyst is exposed to the 1-butene/CO_2 reaction feed, different reactions occur at the same time inside the catalyst bed, namely the oxidative (ODH) and the non-oxidative dehydrogenation (DH) of butenes, the RWGS reaction, 1-butene isomerization, cracking and coking.

In general, the ODH reaction of alkanes both with O_2 and CO_2 is assumed to require a 2-electron reduction of one V(V) to a V(III) or of two- neighboring V(V) to V(IV) and to involve the activation of the C-H bonds of the alkane which is assumed to be the kinetically relevant step [27, 35]. VO_x of high oxidation state can bear both selective as well as non-selective oxygen species [28]. Moreover, it was suggested that ODH of propane with CO_2 can run also over partly reduced VO_x sites [28]. The gas mixture leaving the reactor at short TOS (< 30 min) contained beside BD and butenes also a relatively high amount of CO and cracking products like methane and propene (Fig. S4, Fig. S5). It was found that coke formation was strongest at the early stage of the reaction because at that time the lowest CB were obtained (Fig. 4). Especially, non-selective oxygen species of V(V) oxide seem to be involved in coking and cracking reactions. This assumption is supported by the comparison of the results of the oxidized (as-prepared) and the pre-reduced catalyst. The oxidized Im7.5 produced initially more cracking products and CO (Fig. S5) and revealed a lower initial CB (Fig. S6B) than the pre-reduced catalyst. All catalysts of the Im series reveal an increase in BD formation within the first 30 min TOS (Fig. 2D). It is assumed that here the number of non-selective V(V) oxide species is relatively high leading to a stronger degradation of C4 hydrocarbons and lower initial BD production. An increase in BD production at the early stage was not observed when Gr0.6 or the Aq catalyst were used. On these catalysts side reactions caused by non-selective VO_x species seem to be less strong leading to lower coke amounts (Fig. 13).

With increasing TOS the reduction degree of VO_x is expected to increase because CO_2 is not able to oxidize the reduced VO_x sites completely to their highest oxidation state [24, 28, 38]. BD is formed both by ODH as well as by DH. The DH leads to the formation of BD and hydrogen that can be converted with CO_2 to water and CO in a consecutive reaction (RWGS, Fig. S8). The contribution of reduced VO_x sites to the RWGS reaction has been previously suggested [28]. The RWGS shifts the equilibrium of the DH to the product side and supports the formation of BD. It is believed that the role of the DH in BD formation increases with increasing TOS.

Although the BD yield decreased continuously over time and coke was formed the 1-butene conversion remained at a relatively high level (Fig. 2A, B). The reason for that is the formation of 2-butenes whose yield increased with increasing TOS. At longer reaction times (TOS > 180 min) 2-butenes became the main product (Fig. 3A, B). Considering the catalytic performance of the bare support (Fig. S2) it can be noted that besides SiO_2 surface sites also VO_x sites are involved in the isomerization reaction. The reason for the increasing selectivity of 2-butenes with increasing TOS might be the increasing amount of reduced VO_x sites. It is known that V(IV) and V(III) are Lewis acidic while V(V) does not possess Lewis acidity [34]. Presumably, an increase in the amount of Lewis acid sites is beneficial for double bond isomerization. When water is added to the educt feed much less CO is detected in the product stream (Fig. S3A) while the hydrogen flow increases only moderately (Fig. S3B) indicating that water inhibits rather CO formation than its consumption *via* RWGS. This means that the ODH is more hindered than the DH. Presumably, the water molecule inhibits the re-oxidation of reduced VO_x by reversible adsorption. Therefore, the reduction degree and the acidity of the VO_x is assumed to be higher when water is added. Thus, selectivity of 2-butenes increases (Fig. 3C). The higher selectivity of *cis*- compared to *trans*-butene is probably due to the thermodynamic preference of the latter.

CO_2 conversion is depicted in Fig. 5. The highest conversion was achieved at the beginning of the experiment. In general, CO_2 could be consumed by: 1) re-oxidation of reduced VO_x sites [25, 28], 2) reaction with hydrogen produced by DH (RWGS reaction) [25, 28] or cracking, 3) reaction with carbonaceous deposits [28, 39]. When CO_2 is replaced with nitrogen, ODH can only occur at the very beginning of the reaction (Fig. 6B, Fig. S4). Therefore, BD is almost exclusively formed by DH which cannot be supported by the RWGS. Thus, the BD yield was significantly lower. [28, 39]. Reasons for the higher 1-butene conversion in absence of CO_2 were the increasing number of cracking products, a stronger coke formation, and a faster transformation rate of 1- or 2-butenes to *iso*-butene.

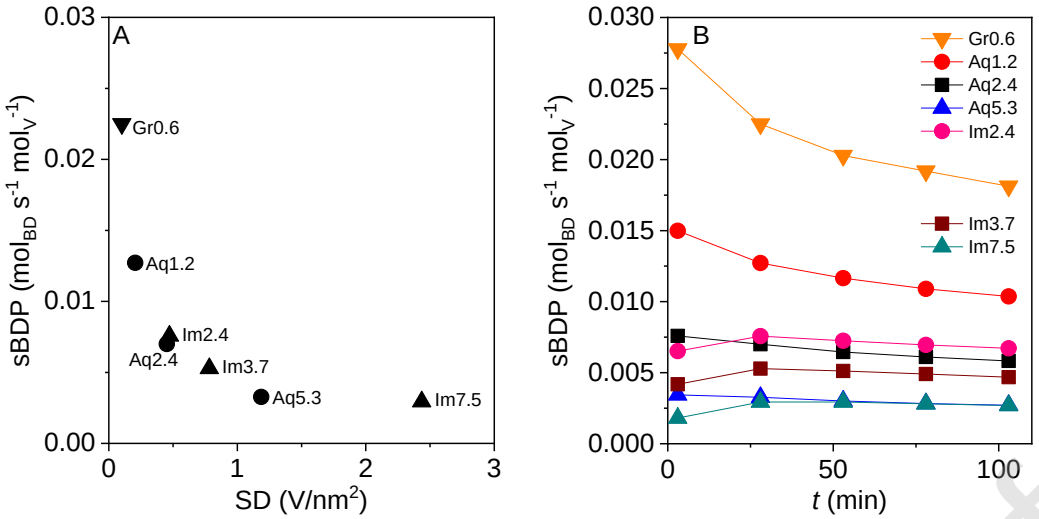

Fig. 14. Specific BD production rate (sBDP) versus A) V surface density (SD) for the different catalysts (TOS = 28 min) and B) TOS.

Fig. 14A reveals the impact of the V surface density (SD) on the specific BD production rate (sBDP), keeping in mind that not all of the VO_x was accessible for the reactants. The highest sBDP (0.023 $mol_{BD} \cdot s^{-1} \cdot mol_V^{-1}$) was obtained for the catalyst with the lowest SD (0.1 V/nm^2) which bears nearly exclusive isolated vanadium sites (Tab. 1). When the catalyst contains additional 2D-polymerized or 3D-VO_x structures, the sBDP decreases significantly although the surface density was only marginally higher. Therefore, it can be concluded that isolated VO_x sites are more efficient in BD formation than two or three-dimensional VO_x domains. In the dehydrogenation of propane under Ar atmosphere isolated VO_x revealed a higher catalytic performance than polymerized and crystalline VO_x [40]. Fig. 13B shows that the values of sBDP are affected by the reaction time, but their relative order does not change. The decrease of sBDP over time is caused by coke formation and probably also by the increasing reduction degree of VO_x.

Due to the two double bonds, BD is assumed to be a better coke precursor than for e.g. butene [22]. With increasing BD production, the amount of coke increases, too (Fig. 13A). Catalysts of the Im series produce relatively high amounts of BD and are more prone to coke formation than the other catalysts. The way coke is formed is influenced by the particular VO_x structure and the distribution of VO_x species on the catalyst surface. The V surface density of Gr0.6 and Aq1.2 is lowest and the distances between the active VO_x sites are larger compared to the distances between VO_x sites on the other catalysts where more VO_x sites (especially more polymerized ones) are present, as indicated in Fig. 8B, Fig. 10. Thus, on Gr0.6 and Aq1.2 BD molecules are

formed on sites which are located relatively far from each other or on VO_x domains which contain only a relatively low number of active VO_x sites. The formation of coke from BD molecules on Gr0.6 and Aq1.2 should occur less readily than on catalysts with higher VO_x surface density or domain size. It can be seen, that much more BD has to be produced on Gr0.6 and Aq1.2 to obtain the same amount of coke like on the other catalysts (Fig. 13B). Noteworthy, Sokolov *et. al.* found VO_x single sites to have the lower coking rates in the dehydrogenation of propane than polymerized VO_x and gave the same explanation for their observations [41].

Finally, the BD formation rate of the VO_x/SBA-15 catalyst was compared with those of other active catalysts which were applied in the dehydrogenation of 1-butene with CO_2 (Tab. S3). As shown, $FeO_x/CeAlO_x$ [20] showed a slightly higher initial activity than VO_x/SBA-15 but its catalytic stability was lower. Moreover, the VO_x/SBA-15 exhibits similar BD formation rate and catalytic stability compared to Cr-SiO_2 [16].

4 Conclusion

The catalytic performance of VO_x species in the dehydrogenation of 1-butene in presence of CO_2 is affected by the support. VO_x species loaded on SBA-15 support possessing high BET surface area and ordered pore structure showed higher BD yields than other supports. On VO_x/SBA-15 catalysts, BD is formed both by oxidative (ODH) and non-oxidative (DH) reaction pathway. CO_2 supports the dehydrogenation reaction by oxidation of reduced vanadium species, by removing hydrogen *via* the RWGS reaction, and by lowering the formation of coke. The extent of ODH and DH on BD formation is assumed to depend on the reaction time. With increasing TOS, the reduction degree of VO_x species increases because CO_2 is not able to re-oxidize reduced VO_x species completely resulting in BD formation mainly by DH. It is assumed that reduced VO_x species are not only involved in DH but also in the isomerization of 1-butene to 2-butenes. The obtained results suggest that VO_x single sites are more efficient in BD formation than polymerized VO_x domains and nanosized crystalline VO_x particles. Beside the reduction of VO_x surface sites, coking is assumed to be the main reason for the catalyst deactivation and the decreasing BD yield with increasing TOS. Both the BD formation and coke formation are affected by the structure of the VO_x species. In the early stage of the reaction, coke formation was strongest. Here, the

reaction of BD or butenes with non-selective oxygen in VO_x sites is assumed to be involved in coke formation.

Author statement

K. I.: Investigation, Methodology, Visualization, Writing- Original draft preparation, Reviewing and Editing **R. E.**: Investigation, Resources **H. L.:** Investigation, Resources **C. K.**: Investigation, Resources; **S. B.**: Investigation, Resources **A. W.**: Investigation, Resources **N. S.**: Supervision, Writing- Original draft preparation, Reviewing and Editing

Declaration of interests

The authors declare that they have no known competing financial interests or personal relationships that could have appeared to influence the work reported in this paper.

5 Acknowledgement

The authors owe thanks to the Leibniz organization for the financial support. Moreover, thanks go to Prof. Sergey Verevkin for providing the thermodynamic data, Dr. Dominik Seeburg and Benny Kunkel for recording the UV-Vis spectra as well as to Dr. Nikolaos Moustakas for helpful discussion.

References

[1] M.R. Allen, D.J. Frame, C. Huntingford, C.D. Jones, J.A. Lowe, M. Meinshausen, N. Meinshausen, Warming caused by cumulative carbon emissions towards the trillionth tonne, Nature, 458 (2009) 1163.

[2] M.D. Porosoff, M.N.Z. Myint, S. Kattel, Z. Xie, E. Gomez, P. Liu, J.G. Chen, Identifying Different Types of Catalysts for CO_2 Reduction by Ethane through Dry Reforming and Oxidative Dehydrogenation, Angew. Chem. Int. Ed., 54 (2015) 15501–15505.

[3] K. Takehira, Y. Ohishi, T. Shishido, T. Kawabata, K. Takaki, Q. Zhang, Y. Wang, Behavior of active sites on Cr-MCM-41 catalysts during the dehydrogenation of propane with CO_2, J. Catal., 224 (2004) 404–416.

[4] F. Zhang, R. Wu, Y. Yue, W. Yang, S. Gu, C. Miao, W. Hua, Z. Gao, Chromium oxide supported on ZSM-5 as a novel efficient catalyst for dehydrogenation of propane with CO_2, Microporous Mesoporous Mat., 145 (2011) 194–199.

[5] C. Wei, F. Xue, C. Miao, Y. Yue, W. Yang, W. Hua, Z. Gao, Dehydrogenation of Isobutane to Isobutene with Carbon Dioxide over SBA-15-Supported Chromia-Ceria Catalysts, Chin. J. Chem., 35 (2017) 1619–1626.

[6] V.D.B.C. Dasireddy, M. Huš, B. Likozar, Effect of O_2, CO_2 and N_2O on Ni–Mo/Al_2O_3 catalyst oxygen mobility in n-butane activation and conversion to 1,3-butadiene, Catal. Sci. Technol., 7 (2017) 3291–3302.

[7] X. Li, B. Yan, S. Yao, S. Kattel, J.G. Chen, T. Wang, Oxidative dehydrogenation and dry reforming of n-butane with CO_2 over NiFe bimetallic catalysts, Appl. Catal. B-Environ., 231 (2018) 213–223.

[8] I. Kainthla, G.V.R. Babu, J.T. Bhanushali, K.S.R. Rao, B.M. Nagaraja, Development of stable MoO_3/TiO_2-Al_2O_3 catalyst for oxidative dehydrogenation of ethylbenzene to styrene using CO_2 as soft oxidant, J. CO_2 Util., 18 (2017) 309–317.

[9] T. Wang, L. Qi, H. Lu, M. Ji, Flower-like Al_2O_3-supported iron oxides as an efficient catalyst for oxidative dehydrogenation of ethlybenzene with CO_2, J. CO_2 Util., 17 (2017) 162–169.

[10] W.C. White, Butadiene production process overview, Chem.-Biol. Interact., 166 (2007) 10–14.

[11] G. Tanimu, A. Palani, S. Asaoka, S. Al-Khattaf, Pore structure effect of support in Ni-Bi-O/mesoporous silica catalyst on oxidative dehydrogenation of n-butane to butadiene, Catal. Today, 324 (2019) 97–105.

[12] E.V. Makshina, M. Dusselier, W. Janssens, J. Degrève, P.A. Jacobs, B.F. Sels, Review of old chemistry and new catalytic advances in the on-purpose synthesis of butadiene, Chem. Soc. Rev., 43 (2014) 7917–7953.

[13] D. Sun, Y. Li, C. Yang, Y. Su, Y. Yamada, S. Sato, Production of 1,3-butadiene from biomass-derived C4 alcohols, Fuel Process. Technol., 197 (2020) 106193.

[14] J.S. Kruger, T. Dong, G.T. Beckham, M.J. Biddy, Integrated conversion of 1-butanol to 1,3-butadiene, RSC Adv., 8 (2018) 24068–24074.

[15] J.Q. Bond, D.M. Alonso, D. Wang, R.M. West, J.A. Dumesic, Integrated Catalytic Conversion of γ-Valerolactone to Liquid Alkenes for Transportation Fuels, Science, 327 (2010) 1110.

[16] B. Gao, Y. Luo, C. Miao, Y. Yue, W. Yang, W. Hua, Z. Gao, Oxidative Dehydrogenation of 1-Butene to 1,3-Butadiene Using CO_2 over Cr-SiO_2 Catalysts Prepared by Sol-gel Method, Chem. Res. Chin. Univ., 34 (2018) 609–615.

[17] W. Yan, Q.Y. Kouk, J. Luo, Y. Liu, A. Borgna, Catalytic oxidative dehydrogenation of 1-butene to 1,3-butadiene using CO_2, Catal. Commun., 46 (2014) 208–212.

[18] B. Yan, Y. Gao, B. Wang, X. Fan, F. Alam, J. Li, T. Jiang, Enhanced Carbon Dioxide Oxidative Dehydrogenation of 1-Butene by Iron-Doped Ordered Mesoporous Alumina, ChemCatChem, 9 (2017) 1–5.

[19] B. Yan, L. Wang, B. Wang, F. Alam, Z. Xiao, J. Li, T. Jiang, Constructing a High-Efficiency Iron-Based Catalyst for Carbon Dioxide Oxidative Dehydrogenation of 1-Butene: the Role of Oxygen Mobility and Proposed Reaction Mechanism, Appl. Catal. A-Gen., 572 (2018) 71–79.

[20] B. Yan, B. Wang, L. Wang, T. Jiang, Ce-doped mesoporous alumina supported Fe-based catalyst with high activity for oxidative dehydrogenation of 1-butene using CO_2 as soft oxidant, J. Porous Mat., 26 (2019) 1269–1277.

[21] W. Yan, Q.-Y. Kouk, S.X. Tan, J. Luo, Y. Liu, Effects of Pt^0-PtO_x particle size on 1-butene oxidative dehydrogenation to 1,3-butadiene using CO_2 as soft oxidant, J. CO_2 Util., 15 (2016) 154–159.

[22] W. Yan, J. Luo, Q.-Y. Kouk, J.E. Zheng, Z. Zhong, Y. Liu, A. Borgna, Improving oxidative dehydrogenation of 1-butene to 1,3-butadiene on Al_2O_3 by Fe_2O_3 using CO_2 as soft oxidant, Appl. Catal. A-Gen., 508 (2015) 61–67.

[23] G. Sun, Q. Huang, S. Huang, Q. Wang, H. Li, H. Liu, S. Wan, X. Zhang, J. Wang, Vanadium Oxide Supported on MSU-1 as a Highly Active Catalyst for Dehydrogenation of Isobutane with CO_2, Catalysts, 6 (2016) 41.

[24] I. Takahara, M. Saito, M. Inaba, K. Murata, Dehydrogenation of propane over a silica-supported vanadium oxide catalyst, Catal. Lett., 102 (2005) 201–205.

[25] Z.-F. Han, X.-L. Xue, J.-M. Wu, W.-Z. Lang, Y.-J. Guo, Preparation and catalytic properties of mesoporous *n*V-MCM-41 for propane oxidative dehydrogenation in the presence of CO_2, Chin. J. Catal., 39 (2018) 1099–1109.

[26] B.P. Ajayi, B.R. Jermy, K.E. Ogunronbi, B.A. Abussaud, S. Al-Khattaf, n-Butane dehydrogenation over mono and bimetallic MCM-41 catalysts under oxygen free atmosphere, Catal. Today, 204 (2013) 189–196.

[27] M.A. Atanga, F. Rezaei, A. Jawad, M. Fitch, A.A. Rownaghi, Oxidative dehydrogenation of propane to propylene with carbon dioxide, Appl. Catal. B-Environ., 220 (2018) 429–445.

[28] I. Ascoop, V.V. Galvita, K. Alexopoulos, M.-F. Reyniers, P. Van Der Voort, V. Bliznuk, G.B. Marin, The role of CO_2 in the dehydrogenation of propane over WO_x–VO_x/SiO_2, J. Catal., 335 (2016) 1–10.

[29] H.R. Patil, Z.V.P. Murthy, A sol–gel route to synthesize vanadium doped silica through ionic liquid control and methylene blue degradation, Chem. Eng. Res. Des., 124 (2017) 134–144.

[30] M. Baltes, K. Cassiers, P. Van Der Voort, B. Weckhuysen, R. Schoonheydt, E. Vansant, MCM-48-Supported Vanadium Oxide Catalysts, Prepared by the Molecular Designed Dispersion of $VO(acac)_2$: A Detailed Study of the Highly Reactive MCM-48 Surface and the Structure and Activity of the Deposited VO_x, J. Catal., 197 (2001) 160–171.

[31] X. Gao, I.E. Wachs, Investigation of Surface Structures of Supported Vanadium Oxide Catalysts by UV−vis−NIR Diffuse Reflectance Spectroscopy, J. Phys. Chem. B, 104 (2000) 1261–1268.

[32] H. Tian, E.I. Ross, I.E. Wachs, Quantitative Determination of the Speciation of Surface Vanadium Oxides and Their Catalytic Activity, J. Phy. Chem. B, 110 (2006) 9593–9600.

[33] K.S.W. Sing, Reporting physisorption data for gas/solid systems with special reference to the determination of surface area and porosity (Recommendations 1984), Pure & Appl. Chem., 57 (1985) 603–619.

[34] U. Rodemerck, M. Stoyanova, E.V. Kondratenko, D. Linke, Influence of the kind of VO_x structures in VO_x/MCM-41 on activity, selectivity and stability in dehydrogenation of propane and isobutane, J. Catal., 352 (2017) 256–263.

[35] X.-L. Xue, W.-Z. Lang, X. Yan, Y.-J. Guo, Dispersed Vanadium in Three-Dimensional Dendritic Mesoporous Silica Nanospheres: Active and Stable Catalysts for the Oxidative Dehydrogenation of Propane in the Presence of CO_2, ACS Appl. Mater. Interfaces, 9 (2017) 15408–15423.

[36] H. Bosch, B.J. Kip, J.G. Van Ommen, P.J. Gellings, Factors influencing the temperature-programmed reduction profiles of vanadium pentoxide, J. Chem. Soc., Faraday Trans. 1, 80 (1984) 2479–2488.

[37] B.P. Payne, M.C. Biesinger, N.S. McIntyre, X-ray photoelectron spectroscopy studies of reactions on chromium metal and chromium oxide surfaces, J. Electron Spectrosc., 184 (2011) 29–37.

[38] H. Fan, J. Feng, X. Li, Y. Guo, W. Li, K. Xie, Ethylbenzene dehydrogenation to styrene with CO_2 over V_2O_5(001): A periodic density functional theory study, Chem. Eng. Sci., 135 (2015) 403–411.

[39] J. Ogonowski, E. Skrzyńska, Deactivation of $VMgO_x$ Catalysts by Coke in the Process of Isobutane Dehydrogenation with Carbon Dioxide, Catal. Lett., 121 (2008) 234–240.

[40] P. Hu, Y. Chen, X. Yan, W.-Z. Lang, Y.-J. Guo, Correlation of the Vanadium Precursor and Structure Performance of Porous VO_X-SiO_2 Solids for Catalytic Dehydrogenation of Propane, Ind. Eng. Chem. Res., 58 (2019) 4065–4073.

[41] S. Sokolov, V.Y. Bychkov, M. Stoyanova, U. Rodemerck, U. Bentrup, D. Linke, Y.P. Tyulenin, V.N. Korchak, E.V. Kondratenko, Effect of VOx Species and Support on Coke Formation and Catalyst Stability in Nonoxidative Propane Dehydrogenation, ChemCatChem, 7 (2015) 1691–1700.